The effect of Variance of Pore Size Distribution on Tortuosity

Nuradeen Labaran Tanko and Auwal Shehu

Abstract— In most literatures, the Heterogeneity of porous media has been shown to depend on geometric properties such as the Pore Size and its Distribution, Pore Connectivity, Pore Shape, Porosity and many more. However, there is no work in the literature to show a clear relationship between characterics properties such as the Pore Size Distribution and Tortuosity. In this work, a simple geometry correlation for Tortuosity of flow path and Pore Size Distribution in porous media is presented. The materials studied are chemically pure mesoporous silica and alumina catalyst support pellets with simplified pore sizes, pore side dsitribution, and surface Chemistry. The Pore Connectivity of the samples are estimated with the aid of Barrett Joyner and Helenda method using a standard technique of Gas Sorption and the Tortuosity from log-attenuation plots by Pulsed Field Gradient Spin-Echoe Nuclear Magnetic Resonance. In conclusion, Macroscopic Tortuosity increases with an increase in the Variance of the Pore Size Distribution of the samples investigated, and thus, in allignment with several two and three dimensional bond networks simulation and Corrugated Pore Structure Models in the literature.

Index Terms - Porous Media, Pulsed Filed Gradient Spin-Echoe NMR, Gas Adsorption Porosimetry, Pore Size Distribution, and Tortuosity

1 INTRODUCTION

Oil reservoirs are physically heterogeneous, with layers of different permeabilities. Therefore, oil reservoirs can contain a network of high permeability fractures surrounded by matrix blocks of low permeability. These heterogeneity can be within and between layers. Effective dispersivity and effective permeability are primarily due to heterogeneity between layer. The permeability of a medium is related to the porosity, but also to the shapes of the pores in the medium and their level of connectedness. The size, shape, and arrangement of conducting spaces in porous materials, such as reservoir rocks, are known to affect the flow of fluids and the displacement of one fluid by another [1,2]. Pores and throats of different sizes may be distributed randomly in a network (randomly heterogeneous) or they may be distributed non-randomly [3]. In the latter case, the larger elements may be clustered together in domains and likewise the smaller elements are clustered together in other domains.

In recent years, [3] compared low-porosity carbonate rocks MicroCT images before and after Mercury intrusion. It was found that ink-bottle shape pores and tortuous complex porous systems prevent Mercury from flowing out of the sample at the end of Mercury porosimetry test. On the other hand, low tortuous cylindrical pores allow Mercury flowing out. In a similar approach, [4] investigated the effect of Tortuosity on capillary imbibition in wetting porous media. The researchers obtained the average height growth of wetting liquid in porous media driven by capillary force. A linear relationship turns out to be the case when dealing with straight capillary tube. [5] expanded [6] work on Tortuosity by investigating by coupling the circle and square models. The researchers established a relationship between tortuosity and porosity with different configurations by using a statistical method. In addition, the tortuosity fractal dimension is expressed as a function of porosity. It was found that tortuosity decreases with an increase in porosity in both cases. Therefore, the predicted correlations of the tortuosity and the porosity agree well with the existing experimental and simulated results which was in good agreement with the work of [7-10]. The pore size distribution (PSD) is one of the most important requirements for predicting tortuosity and entrapment from the retraction curves of Mercury porosimetry. Entrapment is strongly dependent on the topological (pore connectivity and tortuosity) properties of porous media. In recent decades, a direct correlation have been observed between entrapment, PSD, tortuosities, and pore connectivity. For random pore network models of unimodal/monodisperse porous media, simulation results suggest that the mercury entrapment increased as the variance of the PSD got wider [11,12] and decreased with increased pore connectivity [13-15]. Similarly, tortuosity for molecular diffusion is found to increase with decreasing pore connectivity, and increasing width of PSD [16-19].

In a related development, fractal scaling has been applied to soils, both for void and solid phases, as an approach to characterize the porous arrangement, attempting to relate particle-size distribution to soil water retention and soil water dynamic properties [20]. In this approach, the researchers assumed that the void space geometry of soils reflects its solid phase geometry, taking into account that soil pores are lined by the full range of particles, and that their fractal dimension, which expresses their tortuosity, could be evaluated by the fractal scaling of particle-size distribution. The researchers analysed data of 42 soil samples in order to compare fractal dimensions of pore-size distribution. It was found that the Fractal dimensions that reflect the pore trace tortuosity is directly proportional to the PSD. This finding is in good agreement with simulations work of [21-23].

In this paper, a novel multi-technique experimental approach will be used to derive structural-topological relationships in order to understand the mechanism of fluid flow in porous materials. In this regard, this paper will explore this simulation correlation between tortuosity and pore size distribution on a range of porous alumina and silica pellets of spherical or cylindrical geometries. Gas adsorption and mercury porosimetry are complementary methods with the latter covering a much wider size range (0.0035 to 500 μm). There are well-known and standard techniques from gas sorption that can determine key characteristic parameters of porous media, such as the BET Surface area and BJH algorithm for pore size distribution. In the case of mesoporous materials, the Kelvin equation provides a useful model for the transformation of adsorption data into a PSD [24]. There established algorithms based on the Kelvin equation that are used for the determination of PSD such as the Barrett Joyner and Halenda (BJH) method by [25]. However, there are other approaches that consider the fluid-solid interactions [26]. Nevertheless, the BJH method is undoubtedly the most widely accepted method for the analysis of nitrogen adsorption/desorption PSD [24], and thus, it has been adopted in this study. The heterogeneity will be examined with the aid of PGSE NMR. Therefore, the effects from restricted diffusion, and or various domains having different diffusivities, will be investigated. By examining the diffusion behaviour of water within a porous medium, it may be possible to see the changes in tortuosity effects as a function of diffusion time and PSD.

2 THEORY

The study of diffusion by Nuclear Magnetic Resonance (NMR) began back in the early 1950s with the works of [27,28]. Further developments included the use of spin echoes, [28] and stimulated spin echo [29] sequences for studying diffusion coefficients. Most subsequent diffusion sequences are derived from these two sequences [31]. In recent years, the PGSE NRM has been a well-established method for measuring diffusion coefficients in systems ranging from catalyst supports [32-34] porous glasses [35,36] to sedimentary rocks [31,37]. Therefore, the PGSE NMR technique have proven to be powerful and popular tools for diffusion studies in porous media. However, there are a number of challenges that might arise if the investigation is to refer to media of a more complex nature such as the heterogeneous, micro-textured, porous, granular, composite or high-viscosity materials. Consequently, there will be tendencies to anomalous diffusion, superimposed components, extremely small displacement rates, and displacement restrictions [38].

In PGSE NMR, the echo attenuation (R') is defined as the ratio of the echo intensity in the presence of the gradient (I) to the echo intensity obtained in the absence of a gradient (I_0). For unrestricted self-diffusion, where the random motion of the molecules is assumed to follow Gaussian behaviour, the echo intensity (I) is given by [28]:

$$I = I_0 e^{-D\gamma^2 g^2 \delta^2 \left(\Delta - \frac{\delta}{3}\right)}, \quad (1.0)$$

where D is the diffusion coefficient, γ is called gyromagnetic ratio of the observed nucleus, g is the gradient strength, δ is length of the gradient pulse, and Δ is the diffusion time. A range of echo attenuations are obtained by varying g, δ or Δ. Equation 1.0 can be used to calculate diffusion coefficient of the observed nucleus in a homogeneous system. Therefore, in the case of isotropic bulk diffusion, a plot of $\ln\left[\frac{I}{I_0}\right]$ against the group $\xi = \left[\gamma^2 g^2 \delta^2 \left(\Delta - \frac{\delta}{3}\right)\right]$ yields the diffusion coefficient from the slope of the straight line obtained [32]. The diffusion coefficient is obtained by labelling the position of the molecules at the start of the experiment through the use of a field gradient. After a certain period of time (diffusion time, Δ), during which the molecules will have moved to a different random position due to self-diffusion, the positions of the molecules are labelled again by a second gradient [39]. The final signal observed will be a function of the diffusion coefficient D_0, the gradient strength g, δ, and the diffusion time Δ [39]. A typical pulse sequence is illustrated in Figure 1.0

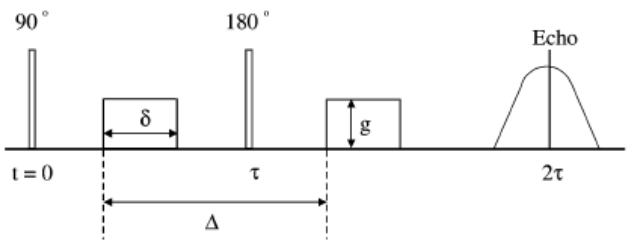

Figure 1.0

A schematic diagram of the pulse sequence that was first introduced by [28]

In general, a linear log-attenuation plot suggests diffusion of a single component in a homogeneous environment and Equation 1.0 describes the relationship between signal attenuation and the diffusion coefficient. The effective diffusion coefficient calculated from a one component fit will be characteristic of the average motion of all molecules and, therefore, will be a combination of free diffusion and restricted diffusion. With a very small value of a short diffusion time (Δ) none of the molecules will be restricted as none of the molecules will have sufficient time to reach the walls of the pores. Therefore, the effective diffusion coefficient measured is that of molecule in free solution.

In contrast, if the diffusion time (Δ) is sufficiently large all the molecules contained within the pores will contact the pore walls and thus undergo restricted diffusion. Consequently, non-linearity in the echo-attenuation plot will be observed if the molecules sample regions associated with largely varying diffusion coefficients. Hence, the long-time behaviour of diffusion coefficient provides an indirect measure of the macroscopic structure [39]. A discrete multicomponent model was derived by [32], Equation 2.0, where the heterogeneity in the apparent diffusion coefficient is attributed to i components, each containing the fraction, p_i, of observed nuclei, with the actual diffusion coefficient, D_i, where ξ is characteristic of the experimental parameters $\left[\gamma^2 g^2 \delta^2 \left(\Delta - \frac{\delta}{3}\right)\right]$

$$I = I_0 \Sigma p_i \exp(-D_i \xi) \quad (2.0)$$

In a PGSE NMR experiment, the diffusion time can be varied from a few milliseconds up to several seconds. Because of effects from the restricting geometry, the measured self-diffusion coefficient (D) depends on the diffusion time (Δ). The measured self-diffusion (D) is also sensitive to physical parameters like permeability and the volume fraction of the diffusing species. The measured self-diffusion (D) can be related to certain characteristics of the porous medium such as the surface-to-volume ratio and the tortuosity (τ). The measured self-diffusion (D) of a diffusing fluid is found to decrease with observation time (Δ) and reaches a plateau value. That plateau value represents the tortuosity (τ) of the system [40].

The effective self-diffusion coefficient (D_{eff}) is a measure of how the water is diffusing within the porous network. Therefore, the tortuosity of a pore network (τ) is a measure of the potential deviation from a linear path that a diffusing molecule may experience. For the diffusion of a liquid in a porous solid, the effective diffusivity of the liquid in the material is related to the molecular self-diffusion coefficient (D_0) of the bulk liquid as follows [32]:

$$D_{eff} = \frac{D_0 \varepsilon}{\tau}, \quad (3.0)$$

where ε voidage of the material. The voidage term is traditionally ignored since the observed signal contains spin density which is directly proportional to voidage. Therefore, Equation (3.0) can be written as:

$$D_{eff} = \frac{D_0}{\tau},$$

(4.0)

where D_0 is the diffusion coefficient of the bulk liquid. Traditionally water is used as the bulk liquid.

In general, tortuosity (τ) describes the geometry of flow paths, thus, a measure of the complexity of a porous medium. It is as a conceptual, dimensionless number representing the departure of a porous system from being composed of straight pores. Since fluid travels along a tortuous path through the medium, the actual or effective pore length (l_{eff}) is greater than the average linear flow path length (l_p). The ratio of the two lengths defines tortuosity [41]. In porous media, tortuosity depends on how well the pores are connected [37].

$$\frac{\text{Effective flow path}}{\text{Average linear flow path}} = \frac{l_{eff}}{l_p} = \tau$$

(5.0)

Furthermore, the total tortuosity (τ) of a porous solid can be considered to have independent contributions from tortuosity on various length scales. The total tortuosity can considered as the product of these independent tortuosities since the effective diffusivity will decrease monotonically with scale [42]. Therefore, the PGSE (NMR) experiment measures:

$$\tau = \tau_e \tau_\mu,$$

(6.0)

where τ_e is the mesoscopic contribution to the tortuosity over length scales of a few pore diameters up to scales at which macroscopic heterogeneities become significant, and τ_μ characterizes tortuosity over length scales of up to a few pore diameters [42]. However, if the molecules diffuse between compact particles, the effective restricted interparticle diffusion coefficient is [37,39],

$$\frac{D_{eff}}{D_0} = \frac{D_{\text{inter}}}{D_0} = \frac{\varepsilon_b}{\tau},$$

(7.0)

where ε_b is the particle bed porosity and τ the tortuosity that the molecules experience diffusion through the bed of particles.

Adsorption pore size distribution analysis of mesoporous materials is based on an adopted interpretation of the mechanisms of capillary condensation, evaporation and the associated hysteresis phenomena [43]. The theory for condensation of vapour into a porous medium is derived from thermodynamic considerations. This is known as the Kelvin equation written as:

$$RT \ln x = \frac{-2\gamma_{LV} V_L \cos(\theta)}{r_K}$$

(8.0)

where r_K is the Kelvin radius.

For nitrogen at liquid nitrogen temperature:

- γ_{LV} is the surface tension of the adsorbate in liquid form = 8.85×10^{-3} N m^{-2};
- V_L = 34.6×10^{-6} m^{-3} mol^{-1};
- R is the universal gas constant= 8.314 J mol^{-1} K^{-1};
- T is the temperature = 77 K;
- θ is the contact angle between the liquid and the wall of the pore = 0°.

Within a porous material, the gas layers continue to fill the pore until the pressure is sufficient that the gas condenses into a 'liquid-like phase'. The pressure at which the gas condenses can be related to the pore size according to the Kelvin equation. However, it becomes less accurate as the PSD becomes smaller because the Kelvin equation is purely thermodynamic, and thus, it does not take account at micropore region [44,45]. This model is usually applied for diameters greater than 2 nm, because below this size the liquid cannot be considered a fluid with bulk properties due to forces exerted by the pore wall. Theoretical calculations suggest that the properties of fluids in microporous structures are highly sensitive to the size of the pores [24].

When the BJH algorithm is used to determine the PSD, the pore size obtained from the Kelvin equation is generally corrected for the multi-layer film thickness using a universal t -layer equation. The empirical observation by [46] have shown that, for many non-porous surfaces, the ratio of the volume adsorbed to the monolayer capacity $\left(\frac{V}{Vm}\right)$ plotted against relative pressure $\left(\frac{P}{P_0}\right)$ all approximately fit a common Type II curve above a relative pressure of 0.3. This implies for a given value of $\left(\frac{V}{Vm}\right)$ the adsorbed layer thickness will be the same regardless of the adsorbent. However, the data used to compile common t -curves was not comprehensive and the universality was only approximated [46]. Therefore, an individual porous solid may show a deviation from the common *t*-curves, as observed experimentally for nonporous templated silicas, such as the SBA-15 using neutron scattering [47]. Nevertheless, the BJH method is undoubtedly the most widely accepted method for the analysis of nitrogen adsorption/desorption PSD [24], and thus, it has been adopted in this study. The BET equation has been used as a standard technique for evaluating the surface area of catalysts. The BET equation derived by [48] for multilayer adsorption is given by:

$$\frac{P}{V(P_0 - P)} = \frac{1}{cV_m} + \frac{c-1}{cV_m}\frac{P}{P_0} \qquad (9.0)$$

A plot of $\frac{P}{V(P_0 - P)}$ against $\frac{P}{P_0}$ yields a line of slope $\frac{c-1}{cV_m}$ and intercept $\frac{1}{cV_m}$. The parameter c indicates the strength of the adsorbent-adsorbate interactions, with $c < 20$ and $c > 100$ representing low and high interaction strength respectively [24]. The BET Equation (9.0) holds for Type I, Type II, Type III and Type IV isotherms,

depending on the nature of the constant C. The selection of the range of relative pressures involving multilayer adsorption is most critical to the evaluation of the surface area of porous solids. [24] have stated that for many materials, the infinite form of the BET Equation (9.0) only fits over a narrow range of relative pressures (typically ~ 0.05 - 0.35).

A coefficient of determination value (R^2) of 0.999 is recommended for most solids [43]. The failure of the BET plot at very low X (X < 0.05) is due to the influence of high adsorption potential in micropores and surface heterogeneity [43]. The BET plot of materials with high microporosity deviates from linearity. This deviation could lead to undesired negative values of the BET constant energy parameter value. Consequently, two criteria have been proposed for the selection of the X range. First, the pressure range must be in the region where $V(P-P_0)$ increases with an increase in X; and second the y - intercept of the linear region must be positive in order to give a meaningful value to BET constant, C [49]. Also, [50] doubt the adsorbed phase is liquid-like.

The BET surface area (a_{BET}) can be evaluated from monolayer capacity by using Equation 10.0, where σ_a is the molecular area of the adsorbate molecule in the completed monolayer and N_A is the Avogadro number. For nitrogen, σ_a is assumed to be 0.162 nm^2. An incorrect nitrogen molecular area can result in an error in the estimation of the surface area. [51] showed that the variation in nitrogen molecular area on different surfaces and quotes a value of 0.162 nm^2 for Al_2O_3 adsorbents.

$$(a_{BET}) = V_m \sigma_a N_A \tag{10.0}$$

The value of σ_a used for nitrogen is based on an assumption that the nitrogen molecules are spherical and rest on a plane surface with a packing similar to that in the bulk liquid. However, nitrogen molecules are in reality non-spherical. They tend to adsorb on the surface in a flat or upright position and also possess a quadrupole moment which causes the nitrogen molecules to adsorb specifically on certain surfaces [52] masking the effect of the formation of a monolayer even though no monolayer has been formed in reality. In addition, the surface chemistry has a strong role in the apparent area projected by adsorbed molecules. Strong interactions can cause the area occupied by each molecule to decrease, and therefore adopt a denser packing relative to weaker interactions between the adsorbent and adsorbate.

2.3 Materials

The materials studied in this work are commercially available, chemically pure mesoporous silica and alumina catalyst support pellets with simplified pore sizes, pore size distribution, and surface chemistry. As highlighted in Table 1, the materials have pore size lying in the range of 7-30 nm. The majority of the materials have unimodal structure with the exception of one bimodal structured material (AL3984T).

Table 1.0
A range of alumina and Silica materials tested

S/N	Sample	Material	Pellet form	Voidage	Nominal diameter (mm)
1	Aerosil	Silica (SiO_2)	Fumed sphere	N/D[a*]	3.5
2	AL3984T	Alumina (Al_2O_3)	Tablet	0.59	3.0
3	AL3992E	Alumina (Al_2O_3)	Extrudate	0.65	3.0
4	C10	Silica (SiO_2)	Gel sphere	0.66	3.0
5	C30	Silica (SiO_2)	Gel sphere	0.69	3.0
6	P7129	Silica (SiO_2)	Gel sphere	0.67	3.0
7	Q17/6	Silica (SiO_2)	Gel sphere	0.49	3.5
8	S980A	Silica (SiO_2)	Gel sphere	0.6	3.0
9	S980G	Silica (SiO_2)	Gel sphere	0.61	2.2
10	Silica Alumina	Silica and Alumina (Al_2O_5Si)	Extrudate	0.60	0.5

Note: a* – Not detected

2.4 Experimental Consideration

2.4.1 Gas Sorption Porosimetry

On each sample, nitrogen sorption experiment was carried out at 77K using a Micromeritics accelerated surface area porosimeter (ASAP) 2010 apparatus. Initially, about 0.2 g of the sample was left under vacuum for 4 hours at a pressure of 0.27 Pa as recommended by [53]. The purpose of the thermal pre-treatment for each sample was to drive any physisorbed water on the sample while leaving the morphology of the sample itself unchanged. The sample tube and its contents were then re-weighed after cooling to room temperature. Thus, the dry weight of the sample before being transferred to the analysis port for the automated analysis procedure was measured.

A full adsorption/desorption micro/mesoporous was carried out since the samples' characteristics were unknown. The calculation of the dead volume of flask (free space analysis) was carried out by using helium. The dead space was the volume of the sample tube excluding the sample itself. As also recommended by [53], equilibration time for the diffusion of nitrogen molecules to access most of the pores present in these materials was set
at forty five seconds.

In the Kelvin Equation $\left[RT\ln x = \frac{-2\gamma_{LV}V_L\cos\theta}{r_k}\right]$, the adsorbate property factor was taken as 9.53×10^{-10} m. Furthermore, it was assumed that, the fraction of pores open at both ends was zero, for both adsorption and desorption. Thus, capillary condensation commenced at the closed end of a pore to form a hemispherical meniscus, and the process of evaporation commenced at a hemispherical meniscus.

- *Dr. Nuradeen Labaran Tanko, Petroleum and Gas Engineering Department, Baze University, Abuja-FCT, Nigeria, Mobile No. +2348067664333. (e-mail: nuradeen.tanko@bazeuniversity.edu.ng).*
- *Auwal Shehu is currently pursuing doctorate degree program in Instrumentation and Control engineering, University of Abuja, Nigeria, Mobile No. +2348066055574. (e-mail: auwal.shehu@bazeuniversity.edu.ng).*

2.4.2 PGSE NMR

The samples were prepared by impregnation with deionised water, under ambient conditions, in a beaker for at least 24 hours. However, before any impregnation, the big pellets, such as Aerosil and Q17/6 tablets, were sliced into appropriate sizes that could readily fit into an NMR sample tube. It was essential to allow the liquid to fully imbibe the porous network. However, excess water was removed from the pellet's external surface by contacting each pellet with pre-soaked tissue paper as demonstrated by [54]. Also, PGSE NMR phenomena are sensitive to the chemical and physical environments of a molecule such as temperature in particular [32]. Therefore, the diffusion coefficient of bulk liquid (deionized water) was measured before and after each sample analysis. This was necessary in order to detect any slight temperature difference. A quartz tube filled with deionised water to a height of around 5 cm was used for estimating the diffusion coefficient, D_0, of the bulk liquid.

All PGSE NMR experiments were performed by using a Bruker AV400 NMR spectrometer, with a broadband (BBO) multinuclear probe equipped with $Z-$ gradient coils. The magnet has static field strength of 9.4 T, yielding a proton resonant frequency of 400.13 MHz for ^1H nucleus. The gradients were supplied by a Bruker Grasp II unit, and the maximum attainable gradient strength was 53.5 G cm^{-1}. The maximum sample length was constrained by the region over which uniform linear gradients could be produced and is 15 ± 1 mm. It was assumed that the magnetic field was uniform and there was no cross-relaxation with the sample. All experiments were conducted at temperatures of 25 ± 0.5 °C. The acquisition parameters used are given in Table 2.0. The data acquisition was controlled by a computer. For the bulk liquid diffusion analysis, acqusition Set 1 was used; where as in the case of sample diffusion analysis, both acquision Sets 1 and 2 were used. A series of eight spectra were taken at increasing gradient strengths and the number of scans for each spectrum was 16. Signal attenuation was used to calculate the diffusion coefficient and comparative tortuosities of the water confined within the samples.

Table 2.0
Experimental acquisition parameters used for PGSE NMR technique

Parameter	Acquisition set	
_	1	2
Gradient strenght, g (G cm^{-1})	0.674 to 32.030	0.674 to 32.030
Diffusion time, Δ (s)	0.05	0.1
Gyromagnetic ratio, γ (radT^{-1}s^{-1})	2.765	2.765
Duration of the gradient, δ (s)	0.02	0.02
Bi polar correction delay, τ_T (s)	0.0001	0.0001

4 Result and Analysis

During the course of Nitrogen Sorption experiments, the problem of batch variability was addressed, and thus, in order to allow for the variation of support structure between pellets from the same batch and to test the reproducibility of measurements, replicate measurements are used. The reported parameters in this section are the mean of these sets used. Moreover, during the course of experiments, the relative pressure was either increased or decreased in small steps, and a small volume of nitrogen, either enters, or leaves, the sample. After each relative pressure change, the volume of nitrogen within the sample was then allowed to come to equilibrium over a period of time. It should be noted that a previous worker [55] within this research group determined the absolute values for different pre-treatment conditions, and the equilibration times suitable for these materials. [55] suggested a pre-treatment condition of 250 °C for 4 hours and 45 seconds equilibration time for the diffusion of nitrogen molecules to access most of the pores present in these materials. This researcher observed that the lower point of the hysteresis loop in most nitrogen isotherms closed at ~ 0.7 to 0.8. This finding was in good agreement with the accepted literature of near equilibration by [52]. Therefore, the same pre-treatment conditions, and equilibration time were adopted in Section 3.0. In the Kelvin Equation (8.0), the adsorbate property factor was taken to be 9.53 × 10^{-10} m. Furthermore, it was assumed that, the fraction of pores open at both ends was zero, for both adsorption and desorption. Thus, capillary condensation commenced at the closed end of a pore to form a hemispherical meniscus, and the process of evaporation commenced at a hemispherical meniscus.

Tables 2.0 presents the BET surface area and variance of the Pore Size Distribution of the investigated materials. The reported uncertainties indicate the spread of the results over samples from the same batch, and the error associated with the technique. It is noteworthy to mention that the result obtained showed strong interactions between the adsorbate and adsorbents $(c>100)$. As detailed in Section 2.0, the surface area of porous media may be determined by using the Brunauer, Emmett and Teller (BET) Equation 9.0. The following pressure range, 0.1 < $x \leq$ 0.3, was used for the BET plots. For each data set, the BET plots yielded a coefficient of determination with linear regression (R^2) greater than 0.999. The BET surface area (a_{BET}) was evaluated from the monolayer capacity by using Equation 10.0. A typical BET surface area plot of one of the samples (Aerosil) is presented in Figure 3.0. Also detailed in Section 2.0, the pressure at which the gas condenses can be related to the pore size according to the Kelvin equation (Equation 8.0). Therefore, the variance of PSD was estimated from the BJH algorithm data.

Also, in this study, tortuosity as a function of diffusion time was investigated. Repeat measurements were made on the bulk probing liquid sample (deionised water) on the same day at constant temperature and yielded diffusion coefficients agreeing to within 0.8 %. For each data set of the probing bulk liquid, the coefficient of determination (R^2) yielded a correlation coefficient greater than 0.999. The self-diffusion coefficient of water at 25 °C was nearly 2.5 ×10^{-9} (± 3.29×10^{-11}) m^2/s in each analysis. The average diffusion coefficient of bulk liquid was considered for calculations. A range of porous alumina and silica pellets of spherical and cylindrical geometry were investigated. In order to allow for the variation of support structure between pellets from the same batch and to test the reproducibility of measurements, replicate measurements were made for all batches. The apparent tortuosity of the samples were calculated by using the diffusion correlation in Equation 4.0. In the case of suspected deviation from linear behaviour, further replicate measurements (up to two repeats) were made to confirm the true nature of the sample. The number of scans was also doubled. The number of scans was increased to ensure better results and consequently reduce the effect of errors associated with measurement, such as the signal to noise ratio. A two component model was used to fit the curve in some of the plots with concave curve characteristic of a heterogeneous sample. The Microsoft Excel Solver was used to estimate the model parameters such as the intensity, diffusivities and their respective fraction in each domain within the sample. These model parameters from Solver were then used as the first guess in Origin 6.1 software to generate better parameters, along with their respective errors.

A minimum of seven fully saturated pellets were probed in each analysis. The data of the sample was subsequently averaged. Therefore, the sample mean error for the tortuosities are given in Table 2.0. The reported uncertainties are the 95% confidence intervals that indicate the

spread of the results over samples from the same batch and the error associated with the PGSE NMR measurement. These uncertainties indicate the reliability of tortuosity estimates for the diffusion times used in this study. Figures 3.0 and 4.0 present the effect of PSD on Tortuosity. It can be seen from Figures 3.0 and 4.0 that there is no clear correlation between Tortuosity and variance of the PSD.

Table 2.0
The average result and standard error obtained from nitrogen adsorption isotherms and PGSE NMR of the samples

	Characterization Technique			
	PGSE NMR		Gas Sorption Porosimetry	
	Tortuosity (τ_{PGSE})		BET Surface area (a_{BET})	Variance of PSD $\left(\frac{\sigma}{\mu}\right)$
Sample	(Δ = 50 ms)	(Δ = 100 ms)		
	(-)	(-)	(m^2g^{-1})	(-)
Aerosil	1.59 ± 0.06	1.86 ± 0.09	162.00 ± 24.00	0.900 ± 0.23
AL3984T	1.75 ± 0.03	1.81 ± 0.04	103.00 ± 9.04	0.722 ± 0.05
AL3992E	1.76 ± 0.02	1.85 ± 0.03	159.00 ± 29.02	0.585 ± 0.04
C10	1.57 ± 0.01	1.63 ± 0.04	326.00 ± 32.56	0.356 ± 0.11
C30	1.41 ± 0.01	1.49 ± 0.05	81.00 ± 4.15	0.190 ± 0.02
Q17/6	2.38 ± 0.03	2.42 ± 0.05	156.00 ± 3.90	0.460 ± 0.09
S980A	1.75 ± 0.02	1.81 ± 0.04	192.00 ± 15.44	0.511 ± 0.16
S980g	1.54 ± 0.02	1.57 ± 0.04	63.00 ± 2.56	0.143 ± N/A
Silica Alumina	2.05 ± 0.04	2.19 ± 0.07	198.00 ± 2.34	1.25 0± 0.50

Furthermore, the tortuosity obtained in Table 2.0 is limited to the length scale probed by the PGSE NMR method. This paper addressed such limitations, and thus, the Macroscopic Tortusity was correlated with the variance of PSD quoted in Table 2.0. The PGSE NMR and MRI studies by [42] provided a more comprehensive study of tortuosity. The combination of these two NMR methods can provide a measure of the macroscopic tortuosity describing the pore structure over length scales of the whole pellet. These researchers investigated some of the samples presented in Table 2.

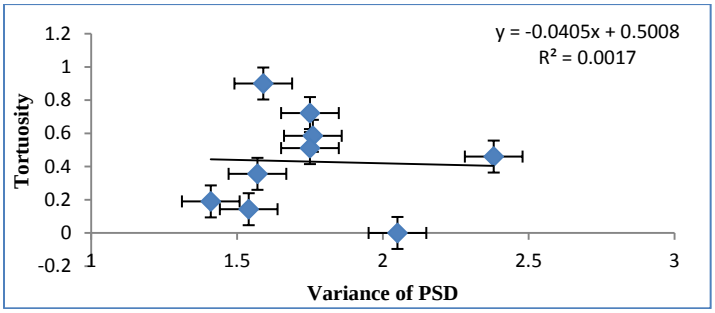

Figure 3.0
Relating the Tortuosity (Δ=50ms) with the Variance of PSD

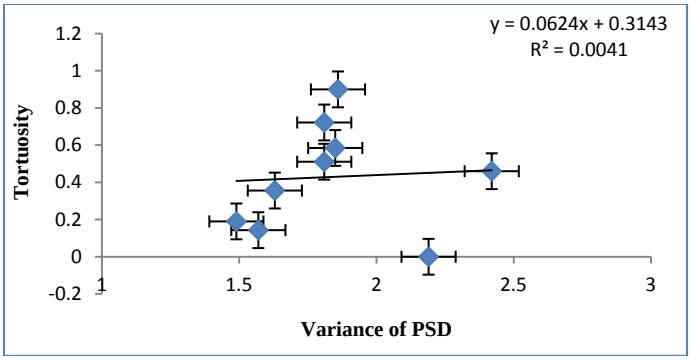

Figure 4.0
Relating the Tortuosity (Δ=100ms) with the Variance of PSD

Table 3.0 presents the Macroscopic contribution to the tortuosity determined by experimental measurements in this study by PGSE NMR and from the MRI work of [42]. For the PGSE (NMR) analysis, a single pellet was suspended over a water reservoir for imbibition for twenty four hours before transfer into the quartz tube. An average of two pellets from the same batch were adopted for this study and the work of [42]. Therefore, the quoted tortuosities in Table 3.0 by [42] are the average values of the fitted distribution diffusivity values. The researchers expressed the macroscopic tortuosity (τ_{Mac}) as a ratio of the tortuosities from the two NMR techniques, and thus, $\tau_{Mac} = \tau_{MRI} / \tau_{PGSE}$. Where τ_{Mac} and τ_{PGSE} are the estimated tortuosities obtained by MRI and PGSE NMR techniques, respectively. Figures 5.0 and 6.0 present the effect of PSD on Macroscopic Tortuosity by PGSE NMR and MRI, respectively. It can be seen from Figures 5.0 and 6.0 that the Tortuosity increases with an increase in PSD.

Table 3.0
Macroscopic contribution to the tortuosity determined by experimental measurements in this study⁺ and from [42]*

	Characterization Method	
	MRI	PGSE NMR
	Macrocopic Tortuosity*	Macroscopic Tortuosity⁺
Sample	(-)	(-)
AL3984E	2.30 ± 0.30	1.28 ± 0.22
AL3992T	2.40 ± 0.30	1.30 ± 0.18
C10	2.30 ± 0.10	1.15 ± 0.06
C30	1.80 ± 0.30	1.09 ± 0.30

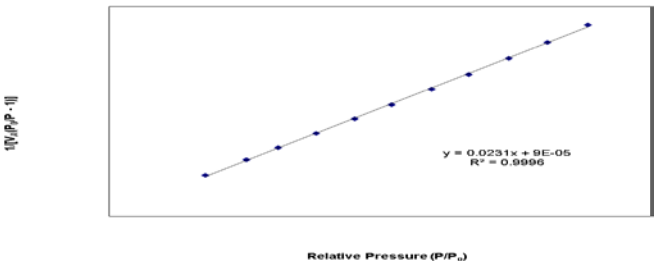

Figure 4.0
The BET plot for Nitrogen adsorption at 77 K of Aerosil

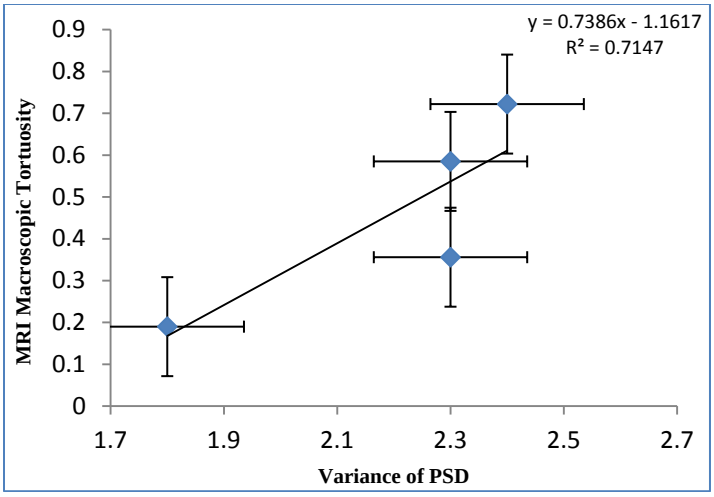

Figure 5.0
Relating the MRI Macroscopic Tortuosity with the Variance of PSD

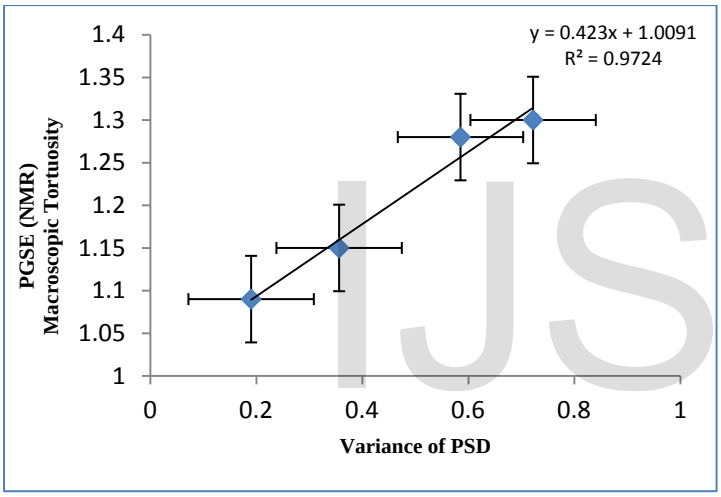

Figure 6.0
Relating the PGSE (NMR) Macroscopic Tortuosity with the Variance of PSD

5.0 DISCUSSION

A novel multi-technique approach has been used to derive structural-topological relationships in order to understand the mechanism of ultimate entrapment in porous materials. As detailed in Section 1.0, several researchers used two and three dimensional bond networks simulation to determine the relationships between structural and transport properties in artificial porous materials. Other workers used basic Corrugated Pore Structure Model (CPSM). Both analytical, basic experimental, and simulation have shown Tortuosity increases with an increase in Pore Size Distribution. It in this regard that this section discusses these correlations for structural-topological relationships that were tested with experimental results for a range of porous alumina and silica pellets of spherical or cylindrical geometries.

In general, within the experimental error, for the different pellets studied from the same batch, the isotherms plotted are of type IV classification according to the IUPAC. This is typical of monolayer–multilayer coverage to capillary condensation pattern, with reproducible type H2 hysteresis loops with mesoporous materials. It should be noted that C30 and S980G have type H2 hysteresis loop, however, due to machine limitations; it was not possible to cause the capillary condensation of liquid nitrogen in pores of sizes greater than mesoporosity. The average pore sizes of C30 and S980G are considerably big and thereby explaining the observed narrower hysteresis loop with very steep and nearly parallel adsorption and desorption branches. This can be explained by the pockets of vapours left in mesopores in C30 and S980G at relative pressures close to unity. Most of the samples investigated have strong interactions between the adsorbate and adsorbents $(c > 100)$. It is likely the surface of these samples exhibit high polarity causing nitrogen molecules to adsorb strongly due to its quadruple moment on certain sites relative to others masking the effect of monolayer formation. [55,56] observed similar findings for some of the material investigated in this study. Therefore, for a cylindrical pore with a narrower neck, capillary condensation could occur by two means. The first being, both cylindrical meniscuses filling at the individual X, determined by the Kelvin equation (Equation 8.0). In the case of advanced condensation effects, both body and throat filling at the filling pressure of the throat exceeds the pressure required to fill the body with a hemispherical meniscus. [57] argued that condensation in a narrow pore might result in the formation of an unstable vapour-liquid interface in the adjacent wider pore that would cause spontaneous condensation in the latter prior to achievement of the limit of metastability of adsorption films. This effect of initiated capillary condensation or advanced condensation may trigger an avalanche filling of the pore network. Consequently, the PSD observed is narrower than it exists in reality for most of the samples investigated in this study.

The application of PGSE NMR diffusion measurements is sensitive to the structure of a medium over a scale comparable to the r.m.s displacement of molecules during the experimental time scale of 10^{-3} to 1 s [31]. The PGSE NMR studies of liquid self-diffusion within porous medium give information on the pore structure itself. Therefore, the diffusion measurements of these materials are the absolute estimated values with respect to the probing bulk liquid (deionised water) used. In addition, the effect of structural damage was limited by cutting the big samples (Aerosil and Q17/6) with a small saw. In general, the PGSE NMR method does not probe length scale equivalent to the dimension of the whole pellet. The method is only limited to the length scale of the probe, and thus, the effect of structural damage in those big samples was negligible in the collected data. Therefore, in order to elucidate transport phenomena in porous media, the interconnectivities of the pore system of a wide range of porous alumina and silica pellets were examined by diffusion over two diffusion time-scales (Δ = 50 and Δ = 100 ms).

The estimated tortuosities of the samples at short diffusion time are of order of 1.85 ± 0.50. At first glance, the estimated tortuosities of most samples varied with diffusion time. Then, 95 % confidence intervals were used to evaluate the reliability of the estimated tortuosities. It was found that the estimated tortuosities did not vary with diffusion time in most samples. [34] observed similar findings for fully saturated silica glasses. However, Aerosil and C30 showed more complex behaviour. The estimated tortuosities of Aerosil and C30 varied with the diffusion time. The complex behaviour of these samples can be attributed to high degree of heterogeneity they possessed than the rest of the samples. Also, the quoted tortuosities of the samples previously studied by [32] and [42] are in good agreement with the estimated tortuosities in Table 2.0. Also, it was found that, for different pellets studied from the same batch of different samples, the estimated tortuosities were in close agreement with minor intra-batch variability in most samples. This observation supports the work of [58]. The observed intra-batch variability could be attributed to slight differences from manufacturing conditions of the material. In addition, the majority of fluid molecules held within a saturated porous medium at short diffusion time would experience free diffusion [59]. However, at long diffusion time, the diffusing molecules would explore the connec-

tivity of the porous medium and the ratio of the apparent diffusion coefficient to the free diffusion coefficient approaches an asymptote equal to the inverse of tortuosity [60].Therefore, the results obtained in this study support the findings of [60] and [59].

Furthermore, the Tortuosity quoted in Table 2.0 was correlated with the variance of Pore Size Distribution. The relationships are presented in Figures 2.0 and 3.0. There was no trend or correlation observed at short and long diffusion time, respectively. The correlation coefficient obtained was 0.001 and 0.004, and thus considered to be statistically insignificant. It is noteworthy to mention that the estimated tortuosities in Table 2.0 describe the interparticle and intrapellet tortuosities. Thus, there was a high possibility of bulk film on the outside of the pellets. Moreover, the tortuosity obtained was limited to the length scale probed by the PGSE NMR method. This research intends to address such limitations.

The PGSE (NMR) in this study and MRI studies by [42] provided a more comprehensive study of tortuosity. The combination of these two NMR methods can provide a measure of the macroscopic tortuosity describing the pore structure over length scales of the whole pellet. In this approach, the effect of intra batch (intraparticle), and extra film thickness of water, to the overall diffusional displacement was investigated. Therefore, the diffusion coefficients measured in this study refer to the molecular self-diffusion coefficient of the imbibed water within the pore space of a single pellet. Also, it was found that, for different pellets studied from the same batch of different samples, the estimated tortuosities were in close agreement with minor intra-batch variability in most samples. This observation supports the work of [58]. The observed intra-batch variability could be attributed to slight differences from manufacturing conditions of the material.

The variance of Pore Size Distribution is correlated with the macroscopic tortuosity quoted in Table 3.0. Figures 5.0 and 6.0 present the relationships between Macroscopic Tortuosity [PGSE (NMR) and MRI] and the variance of Pore Size Distribution, respectively. It can be seen that Macroscopic Tortuosity increases with an increase in the variance of Pore Size Distribution. The Macroscopic tortuosity increase with an increase in the variance of the PSD. To support this correlation, static analysis was carried out in order to rule out any possibility of random chance. A common alpha level for research is 0.10, and was thus adopted in this study [61]. In Figures 5.0 and 6.0, the correlation coefficients obtained for the correlation are 0.715 and 0.972. The number of data points used is four. Therefore, by using the critical value table for Pearson's correlation coefficient [61], it can be concluded that the correlation is statistically significant. This finding verified and is in good agreement with the simulation works of [15-22].

6.0 CONCLUSION

A novel multi-technique approach has been used to predict the relationships between Tortuosity and mercury entrapment. A range of porous alumina and silica pellets of spherical or cylindrical geometries were investigated. Most of the samples have strong interactions between the adsorbate and adsorbent, and thus are susceptible to advanced condensation phenomena that will result in a narrow PSD than it exists in reality. PGSE NMR studies carried out on fully and partially saturated samples revealed similar tortuosities for the range of length scales studied. Initial attempt to correlate Tortuosoity and variance of PSD was statistically insignificant due to the tortuosity obtained was limited to the length scale probed by the PGSE NMR method. This paper address such limitations, and thus, the variance of Pore Size Distribution was correlated with the macroscopic tortuosity by PGSE (NMR) and MRI, respectively. The combination of these two NMR methods can provide a measure of the macroscopic tortuosity describing the pore structure over length scales of the whole pellet. It was found that the Macroscopic increase with an increase in the Variance of PSD as observed in several two and three dimensional bond networks simulation and Corrugated Pore Structure Models (CPSM).

ACKNOWLEDGMENT

The authors thanks Professor S.P. Rigby for his valuable discussion in this research.

REFERENCES

[1] Tsakiroglou C. D., Payatakes A. C., 1998. Mercury Intrusion and Retraction in Model Porous Media, *Adv. Colloid Interf. Sci*., 75, 215–253.

[2] Dullien, F.A.L., 1992. *In porous media; Fluid transport and pore structure*. 2nd edition. New York: Accademic press.

[3] Fusi, N., and Martinez, J.M, 2013. Mercury porosimetry as a tool for improving quality of micro-CT images in low porosity carbonate rocks. *Engineering Geology*, 166, 272-282.

[4] Cai, J., and Yu, B., 2011. A Discussion of the Effect of Tortuosity on the Capillary Imbibition in Porous Media. *Transport in Porous Media*, 89(2), 251–263.

[5] Jian-Long, K., Xue-Ming,T., Hai-Yan, Z., Hang-Jun, L., Feng-Min, W., You-Sheng, X., and Yong-Sheng, D. Tortuosity for streamlines in porous media. Chin. Phys. B, 2011, Vol. 21, No. 4, 044701.

[6] Matyka, M., Khalili, A., and Koza, Z. Tortuosity-porosity relation in porous media flow. *Physical Review E* 78, 2008, 026306.

[7] Fernie, S., and Latief, F.D.E. Tortuosity–Porosity Relationship in Two-Dimensional Fractal Model of Porous Media. *Fractals*, 2013, 21, 1350013.

[8] Lu, L., Yu, B., Cai, J., Xeng, X. Numerical Simulation of Tortuosity for Fluid Flow in Two-Dimensional Pore Fractal Models of Porous Media. *Fractals* 22, 2014, 1450015.

[9] Duran, L., Hernandez, A., Holek, S. Relation between the porosity and tortuosity of a membrane formed by disconnected irregular pores and the spatial diffusion coefficient of the Fick-Jacobs model. *Physical Review E*, 95, 2010, 052804.

[10] Androutsopoulos, G.P. and Mann, R., 1979. Evaluation of mercury porosimeter experiments using a network pore structure model. *Chemical Engineering Science*, 34, 1203-1212.

[11] Portsmouth, R.L., and Gladden, L.F., 1991. Determination of pore connectivity by mercury porosimetry. Chemical Engineering Science, 46 (12), 3023-3036.

[12] Portsmouth, R.L., and Gladden, L.F., 1992. Mercury porosimetry as a probe of pore connectivity. *Chemical Engineering Research and Design*, 70 (1), 63-70.

[13] Friedman, S.P., Zhang L., Seaton, N.A., 1995. Gas and Solute Diffusion Coefficients in Pore Networks and its Description by a Simple Capillary Model. *Transport in Porous Media*, 19 (3), 281-301.

[14] Vogel, H.J., 1997. Morphological determination of pore connectivity as a function of pore size using serial sections. European Journal of Soil Science, 48, 365–377.

[15] Vogel, H.J., 2000. A numerical experiment on pore size, pore connectivity, water retention, permeability, and solute transport using network models. *European Journal of Soil Science*, 51, 99–105.

[16] Armatas, G.S., and Pomonis, P.J., 2004. A Monte Carlo pore network for the simulation of porous characteristics of functionalized silica:

pore size distribution, connectivity distribution and mean tortuosities. *Chemical engineering science*, 59, 5735-5749.

[17] Armatas G.S, Salmas CE, Louloudi M., Androutsopoulos G.P., Pomonis, P.J., 2003. *Relationships among pore size, connectivity, dimensionality of capillary condensation, and pore structure tortuosity of functionalized mesoporous silica.* Langmuir 19 (8), 3128-313.

[18] Armatas, G.S., 2006. Determination of the effects of the pore size distribution and pore connectivity distribution on the pore tortuosity and diffusive transport in model porous networks. *Chemical engineering science*, 61, 4662 – 4675

[19] Bacci, O.O.S, Reichardt, K., Villa-Nova, 1996. Relation Hydraulic Conductivity. *Science Agriculture*, 53, 2-3.

[20] Pomonis, P.J., Kolonia, K.M., Artmas, G.S., 2001. Relationship between Pore Connectivity and Mean Pore Size in Modulated Mesoporous Vanado-Phosphoro-Aluminates and Some Similarities with the Branching of Trees. *Langmuir*, *17* (26), 8397–8404.

[21] Vervoort, R.W., and Cattle, S.R., 2003. Linking hydraulic conductivity and tortuosity parameters to pore space geometry and pore-size distribution. *Journal of Hydrology*, 0022-1694.

[22] Sepehr Sadighi, S., Majid Bahmani, M., Reza, S., Mohadecy, S., 2013. Effect of Pore Size Distribution and Temperature on the Catalyst Tortuosity. *Chemical Engineering Research Bulletin*, 16, 61-72.

[23] Rouquerol, F., Rouquerol, J., and Sing, K., 1999. *Adsorption By Powders And Porous Solids Principles, Methodology And Applications*. London: Academic Press.

[24] Barrett, E. P., Joyner, L. G., Halenda, P. P., 1951. The determination of pore volume and area distributions in porous substances. I. Computations from nitrogen isotherms, *J. Am. Chem. Soc.*, 73, 373–380.

[25] Horvath, G., and Kawazoe, K., 1983. Method for calculation of effective pore size distribution in molecular sieve carbon. *J. chem. Engng Japan*, 16, 470-475.

[26] Hahn, E.L., 1950. Spin echoes. *Physical review*, 80 (4).

[27] Conner, W.C., and Lane, A.M., 1984. Measurement of the morphology of high surface area solids: Effect of network structure on the simulation of porosimetry. *Journal of Catalysis*, 89 (2), 217-225.

[28] Stejskal, E. O., and Tanner J.E., 1965. Spin diffusion measurements: spin echoes in the presence of a time dependent field gradient. *Journal of Chemical Physics*, 42,288 -292.

[29] Tanner, J. E., 1970. Use of the stimulated echo in NMR diffusion studies. *J. Chem. Phys.*, 52, 2523–2526.

[30] Callaghan, P. T., 1984. Pulsed field gradient nuclear magnetic resonance as a probe of liquid state molecular organisation. *Aust. J. Phys.*, 37, 359-387.

[31] Hollewand, M.P., and Gladden, L.F., 1995a. Transport heterogeneity in porous pellets-I. PGSE NMR studies. *Chemical Engineering Science*, 50, 309-326.

[32] Rigby, S.P., 1999. NMR and modelling studies of structural heterogeneity over several lengthscales in amorphous catalyst supports. *Catalysis Today*, 53 (2), 207-223.

[33] Farrher, G., Ardelean, I., Kimmich, R., 2008. Time-dependent molecular diffusion in partially filled porous glasses with heterogeneous structure. *Applied magnetic resonance*, 34 (1-2), 85-99.

[34] Pimenov, G.G., and Skirda, V.D., 2005. NMR Study of the Kinetics of Butane and Hexane Adsorption from Vapour Phase by Porous Glasses. *Colloid Journal*, Vol. 67(6), 746–750.

[35] Nechifor, R., Badea, C., and Ardelean, I., 2009. Nuclear magnetic resonance studies of liquids morphology inside partially saturated porous media. *Journal of physics: conference series*, 182 (1).

[36] Kleinberg, R.L., Kenyon W.E., and Mitra P.P., 1994. Mechanism of NMR relaxation of fluids in rock. *Journal of magnetic resonance series A*, 108, 206-214.

[37] Ardelean, I., and Kimmich, R., 2003. Principles and unconventional Aspects of NMR Diffusometry. *Annual Reports on NMR Spectroscopy*, 49,43-115.

[38] Veith, S.R, Hughes, E., Vuataz, G., and Pratsinis, S.E. Restricted diffusion in silica particles measured by pulsed field gradient NMR. *Journal of Colloid and Interface Science*, 2004, 274, 216–228

[39] Latour, L.L., Kleinberg, R.L., Mitra, P.P., Sotak, C.H. Pore-Size Distributions and Tortuosity in Heterogeneous Porous Media. *Journal of Magnetic Resonance*,1995, Series A, Vol. 112, 83-91.

[40] Scholes, O.N., Clayton, S.A., Hoadley, A.F.A, and Tiu, C. Permeability anisotropy due to consolidation of compressible porous media. *Transport porous media*. 2007, 68 365-387.

[41] Rigby, S.P., and Gladden, L.F., 1998. The use of magnetic resonance images in the simulation of diffusion in porous catalyst support pellets. *Journal of Catalysis*, 173 (2), 484-489.

[42] Sing, K.S.W., Everett, D.H., Haul, R.A.W., Moscou, L., Pierotti, R.A., Rouquerol, J. and Siemieniewska, T., 1985. Reporting physisorption data for gas solids systems with special reference to the determination of surface area porosimetry and porosity (recommendation 1984). *Pure and applied chemistry*, 57, 603-619.

[43] Seaton, J., 1989. Cultural Conservatism, Political Radicalism, 1989. *The Journal of American Culture*, 12 (3), 1-10.

[44] Lastoskie, C., Gubbins, K.E., Quirke, N., 1993. Pore size distribution analysis of microporous carbons: a density functional theory approach. *J. Phys. Chem.*, 97 (18), 4786–4796.

[45] Rigby, S.P., Chigada, P.I., Perkins, E.L., Lowe, J., Edler, K.J., 2008. Fundamental studies of gas sorption within mesopores situated amidst inter-connected, irregular network. *Adsorption-journal of the international adsorption society*, 14 (2-3), 289-307.

[46] Schreiber, J.F., Grüner, F., Schramm, U., Geissler, M., Schnürer, M., Ter-Avetisyan, S., Hegelich, M., Cobble, J., Brambrink, E., Fuchs, J., Audebert, P., and Habs, D., 2006. Analytical Model for Ion Acceleration by High-Intensity Laser Pulses. *Phys. Rev. Lett*., 97.

[47] Brunauer, S., Emmett, P. H., and Teller, E. 1938. Adsorption of Gases in Multimolecular Layers. *Journal of the American Chemical Society*, 60, 309-319.

[48] Rouquerol, J., Llewellyn, P., and Rouquerol, F., 2007. *Is the BET Equation Applicable to Microporous Adsorbents?*. Amsterdam: Elsevier.

[49] Gregg, S. J., and Jacobs, J. 1948. An examination of the adsorption theory of Brunaeur, Emmett & Teller and Brunaeur, Deming, Deming & Teller. *Trans. Faraday Soc*. 44, 575.

[50] Karnaukhov, A.P., 1985. Improvement Methods for Surface Area Determinations. *Journal of Colloid and Interface Science*, 103 (2), 311-320.

[51] Gregg, S.J., and Sing, K.S.W., 1982. *Adsorption, Surface Area and Porosity*. London: Academic Press.

[52] Evbuomwan, O.E. *The structural characterisation of porous media for use as a model reservoir rocks, adsorbents and catalyst*. Thesis (PhD). University of Bath. 2009.

[53] Hollewand M.P., Gladden L.F. Heterogeneities in structure and diffusion within porous catalyst support pellets observed by NMR Imaging. *Journal of catalyst*, 1993, 144, 254-272

[54] Rigby, S.P., Watt-Smith, M.J., Fletcher, R. S., 2004. Simultaneous determination of the pore-length distribution and pore connectivity for porous catalyst supports using integrated nitrogen sorption and mercury porosimetry. *Journal of catalysis*, 227 (1), 68-76.

[55] Rigby, S.P., and Chigada, P.I., 2009. Interpretation of integrated gas sorption and mercury porosimetry studies of adsorption in disordered networks using mean-field DFT. *Adsorption-journal of the international adsorption society*, 15 (1), 31-41.

[56] Neimark, A.V., 1991. Percolation theory of capillary hysteresis phenomena and its applications for characterization of porous solids. *Studies in surface science catalysis*, 62, 67-74.

[57] Karger, J., and Ruthven, D.M., 1992. *Diffusion in Zeolites and other Microporous Solids*. John Wiley.

[58] Lafitte, G., Söderman, O., Thuresson, K., Davies, K., 2007. PFG-NMR diffusometry: A tool for investigating the structure and dynamics of noncommercial purified pig gastric mucin in a wide range of concentrations. Biopolymers, 86 (2), 165-175.

[59] Sen, P.N., Schwartz, L.M., Mitra, P.P., 1994. Probing the structure of porous media using NMR Spin echoes. *Magnetic resonance imaging*, 12 (2), 227-230.

[60] Chatfield, C., 1983. *Statistics for technology: A course in applied statistics*. Chapman & Hall/CRC.